Fungal Ecology 57-58 (2022) 101155

Contents lists available at ScienceDirect

Fungal Ecology

journal homepage: www.elsevier.com/locate/funeco

Crown closure affects endophytic leaf mycobiome compositional dynamics over time in *Pseudotsuga menziesii* var. *menziesii*

Kyle A. Gervers [a,*], Daniel C. Thomas [b], Bitty A. Roy [c], Joseph W. Spatafora [a], Posy E. Busby [a]

[a] Department of Botany and Plant Pathology, Oregon State University, Corvallis, OR, 97333, USA
[b] Department of Ecological Microbiology, Bayreuth Center of Ecology and Environmental Research (BayCEER), University of Bayreuth, Bayreuth, 95440, Germany
[c] Institute of Ecology and Evolution, University of Oregon, Eugene, OR, 97403, USA

ARTICLE INFO

Corresponding Editor: James White

Keywords:
Nothophaeocryptopus
Rhabdocline
Fungi
Endosphere
Old-growth
Community ecology
ITS
Metabarcoding
Airborne LiDAR

ABSTRACT

Old-growth *Pseudotsuga menziesii* var. *menziesii* forests produce complex environmental and spatial gradients along which biota assemble. Given this, it has been proposed that changes in the crown microenvironment are associated with different community assembly outcomes for needle fungi. Using high-throughput sequencing, the endophytic mycobiomes of needles were characterized for increasing ages of needles sampled along the boles of eight coastal Douglas-fir trees. Leveraging airborne light detection and ranging (LiDAR) data to create three-dimensional "point cloud" representations of tree crowns revealed that crown closure accounted for more fungal compositional variation than height in crown, and fungal richness and diversity were positively correlated with increasing crown closure. Supplementing the point clouds of each climbed tree with clouds from >5,000 randomly selected trees in the study area showed that fungal communities from closed portions of the crown were increasingly structured with needle age. These findings highlight the importance of the crown microenvironment in the development of foliar fungal communities for a foundation tree species.

1. Introduction

Endophytic fungi live a significant part of their life cycles within their hosts without producing symptoms of disease (Saikkonen et al., 1998). Those that infect plant leaves are generally horizontally transferred between host plants, comprise a diverse taxonomic and phylogenetic assemblage of fungi, and can modulate foliar disease severity (Busby et al., 2016), stomatal conductance (Arnold and Engelbrecht, 2007), and nutrient uptake (Christian et al., 2019). Given the functional importance of foliar fungal communities for regulating plant responses to biotic and abiotic stresses, elucidating the factors controlling their composition will have important implications for both basic and applied plant sciences.

Communities of foliar endophytic fungi vary along environmental gradients at landscape (Zimmerman and Vitousek, 2012) and regional (Barge et al., 2019) scales, yet there are few studies examining patterns of fungal community variation along the vertical axis of individual host plants (Osono and Mori, 2004; Harrison et al., 2016; Izuno et al., 2016; Oono et al., 2017). While this omission may be inconsequential for annuals and plants of modest stature, the crowns of tall, old-growth conifer species like *Pseudotsuga menziesii* var. *menziesii* support vertically stratified ecological communities in which compositions change with height in crown (McCune, 1993; Sillett and Rambo, 2000). And although *P. menziesii* crowns were among the first rigorously sampled for endophytic needle fungi (Sherwood and Carroll, 1974), further characterization of these endophyte communities with modern sequencing techniques is needed.

Tree crowns span multiple microclimatic gradients. UV-B and photosynthetically active radiation are abruptly attenuated by foliage in the mid-crown (Parker, 1997), while the upper crown is only intermittently wet, with generally warmer and less stable air temperatures than the lower portions of the crown that are buffered by vegetation (Heffernan, 2017). Further, unshaded foliage can become nearly 7 °C warmer than surrounding air temperatures, while leaf temperatures of shaded foliage are relatively stable (Doughty and Goulden, 2008). These and other microclimatic factors can also affect fungal colonization potential in other contexts (Carisse et al., 2000; Unterseher and Tal, 2006; Norros et al., 2015), and may also influence foliar mycobiome composition by acting as environmental filters dependent on the degree of canopy openness (Gilbert et al., 2007). Additionally, foliage at different heights in the crown possesses different morphological, physiological, and spectral properties (Ishii et al., 2002; Gebauer et al., 2015;

* Corresponding author.
E-mail address: gerversk@oregonstate.edu (K.A. Gervers).

https://doi.org/10.1016/j.funeco.2022.101155
Received 20 September 2021; Received in revised form 24 March 2022; Accepted 26 March 2022
Available online 28 April 2022

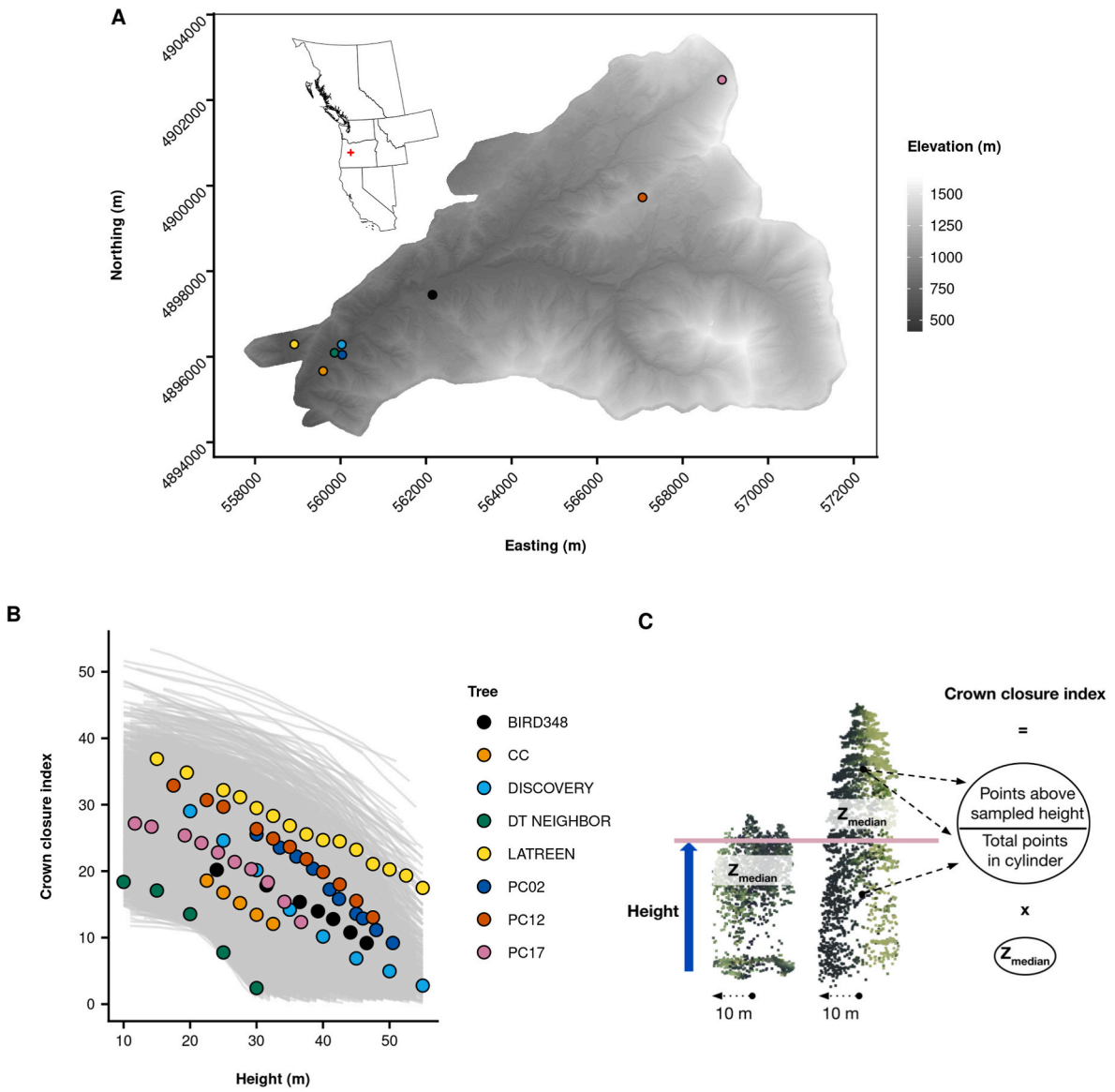

Fig. 1. Locations of the H.J. Andrews Experimental Forest (HJA) and the climbed and sampled trees (A). The inset and the red cross indicate the center position of HJA within the North American Pacific Northwest. The positions of sampled trees have been jittered (±150 m) to avoid overlap. The map is based on a digital terrain model from Spies, 2016. Relationship between height in crown and crown closure (B). Grey lines show data from point clouds associated with 5828 trees randomly sampled across HJA (each with randomly sampled crown heights), while colored lines and points represent point clouds associated with trees that were climbed and sampled as part of this study. Point cloud cylinders are centered on the treetop of a focal tree, but include all point returns within a 10 m radius (C). Although the same vertical height can be sampled in two different trees, these heights can be associated with different crown closure indices.

Schweiger et al., 2020), potentially allowing host-mediated, within-crown biotic filtering of needle communities. Because *P. menziesii* canopy foliage can be long-lived, community assembly outcomes for the canopy mycobiome at a point in time may have lasting impacts on future community structure and assembly as foliage is exposed to infection over time (Bernstein and Carroll, 1977; Arnold and Herre, 2003; Osono, 2008).

The potential for light detection and ranging (LiDAR) point cloud data to account for variation in the diversity and composition of terrestrial fungal communities (Peura et al., 2016; Thers et al., 2017; Valdez et al., 2021) and to characterize the habitat preferences of crown-dwelling organisms (Barnes et al., 2016) has recently been demonstrated. These and other approaches rely on LiDAR technologies, which associate several emitted and detected laser pulse echoes ("returns") with accurately recorded positions. Further processing yields three-dimensional "point clouds'', with each point in space representing a position where the laser pulse reflects off vegetation or other surfaces. Researchers can then obtain accurate estimates of canopy height, cover, and structure to inform their analyses of communities (Lefsky et al., 2002). LiDAR-derived metrics also correlate with specific aspects of the microclimate such as near-surface air temperatures in old-growth *P. menziesii* forests (George et al., 2015; Frey et al., 2016; Davis et al., 2019). Thus, combining mycobiome data with a co-localized measurement of the crown microenvironment may help to elucidate how endophyte communities vary along tree stems and among trees. Here, point cloud data derived from airborne LiDAR and high-throughput amplicon sequencing data were leveraged to test the hypothesis that the composition and diversity of fungal needle endophyte communities are correlated with crown exposure. In addition to examining the height above ground as a compositionally relevant factor, our definition of exposure considered an airborne LiDAR-derived measure of crown closure, which quantifies the amount of intervening foliage (measured as "points" in a point cloud) between the sky and a specified height in the tree. Altogether, positions in the crown that are further from the

ground and less obscured by foliage are more exposed; positions closer to the ground and more obscured by foliage (more closed) are less exposed. We further explored the relevance of exposure as a concept and hypothesized that more- or less-exposed crowns undergo different shifts in community structure with each age class of needle, potentially reflecting differences in needle endophyte community assembly. We report that only closure uniquely contributed to an ecologically informed metric of exposure, accounting for variation in community composition and diversity, and exposure groups showed differing patterns in community structure over the needle ages sampled.

2. Methods

2.1. Sampling and surface sterilization

Six trees (BIRD348, CC, LATREEN, PC02, PC12, and PC17) at the H. J. Andrews Experimental Forest (HJA, Fig. 1) were sampled in late winter 2016–2017, and two other trees (DISCOVERY and DT NEIGHBOR) were sampled in winter 2017–2018. HJA is located on the west side of the Cascade Range of central Oregon; its 6400 ha range from 410 to 1630 m in elevation, and canopies can exceed 93 m in height. Using single-rope climbing techniques (Video S1), where possible, accessible branches from opposing aspects were sampled every 1–5 m in each tree, and the height of each sample collection above ground level was noted. Collection of branches began with the first available branch closest to the ground, and continued as high as could be safely climbed. Due to safety concerns, climbing did not reach the tops of tree crowns. Branches were transported in coolers with ice blocks and then later refrigerated at 4 °C until they could be processed (within 72 h). Needles that experienced one (A1), two (A2), three (A3), and four (A4) growing seasons were sampled from each branch and represented four unique needle age classes. To target endophytic fungi, needles were surface sterilized via immersion in 70% ethanol for 1 min, 4 min in 5% sodium hypochlorite, 1 min again in 70% ethanol, followed by a sterile distilled water rinse before being frozen at −80 °C (modified from Thomas et al., 2016). Needles from different aspects at a given height on each tree were pooled prior to 72 h of lyophilization. Each sample consisted of a unique tree-by-height-by-age combination (71 heights x 4 ages = 284 samples).

Supplementary data related to this article can be found at https://doi.org/10.1016/j.funeco.2022.101155.

2.2. DNA extraction, Illumina MiSeq sequencing, and sequence processing

DNA was extracted using OPS Diagnostics' 96 Well Synergy™ Plant Homogenization plates (Lebanon, New Jersey, USA). Each well received five needles of a single age class, sourced from each sampled height; empty wells were processed per the kit instructions and served as extraction controls. To reduce PCR inhibition issues, DNA extractions were cleaned with 1.2X volumes of Mag-Bind® TotalPure NGS magnetic beads (Omega Bio-Tek, Norcross, Georgia, USA). The ITS2 region was amplified in a primary PCR using the 5.8S-Fun and ITS4-Fun fungal-specific primers (Taylor et al., 2016) Each primer consisted of sequences that amplified the ITS2 region, followed by 3–6 bp length heterogeneity spacers, and subsequently terminated with an Illumina adapter sequence. 25 μl PCRs were carried out with MyTaq™ HS Red Mix (Meridian Bioscience, Inc., Cincinnati, Ohio, USA), 0.4 μM of each primer, 5 μl of template, and applying the following cycling parameters: 3 min denaturation at 95 °C, 28 cycles of 95 °C (30 s), 58 °C (30 s), 72 °C (30 s), followed by a 2 min extension at 72 °C. Using a secondary PCR, sample barcodes and Illumina flow cell adapters were then incorporated into these PCR products after amplification was visually confirmed via agarose gel electrophoresis. 25 μl PCRs were carried out with MyTaq™ HS Red Mix, 0.5 μM of each barcode primer, 1 μl of template, and with the following cycling parameters: 3 min at 95 °C, eight cycles of 95 °C (30 s), 55 °C (30 s), 72 °C (30 s), followed by a 2 min extension at 72 °C. This PCR product was purified and normalized (to 2.5–3.0 ng μl^{-1}) using Charm Biotech's Just-a-Plate™ 96 Well Purification and Normalization plates (Cape Girardeau, Missouri, USA) and submitted the library to the Center for Genome Research and Biocomputing (Oregon State University, Corvallis, Oregon) for 2 × 300 paired end sequencing on the Illumina MiSeq platform (Reagent Kit v3, San Diego, California, USA).

Reads were demultiplexed with Pheniqs (Galanti et al., 2017) and adapters were trimmed using Cutadapt (Martin, 2011) and SeqPurge (Sturm et al., 2016). Reads were then denoised, filtered of chimeras, and merged using the DADA2 R package (Callahan et al., 2016), producing amplicon sequence variants (ASVs) using the pseudo-pooling method. ITS2 sequences were extracted with ITSx (Bengtsson-Palme et al., 2013) and were aligned to the 2020-02-04 UNITE eukaryote release (singletons included, Abarenkov et al., 2020a) with VSEARCH (Rognes et al., 2016). If at least half of each ASV's global alignments (at > 0.5 identity) were fungal, the ASV was retained as a putative fungal sequence. The LULU R package, implementing the LULU algorithm, was used to collapse potentially infragenomic or artifactual ASVs into OTUs (Frøslev et al., 2017), with minimum match = 97% similarity, and minimum relative occurrence = 95%. Although not all ASVs were affected by this approach, putative taxa will be referred to as OTUs. After this step, OTUs for which >1% of non-control reads were found in the extraction and PCR controls were identified as contaminants and removed. Taxonomy was then assigned to the remaining subset of OTUs using the fungal version of the 2020-02-04 UNITE release (without singletons, Abarenkov et al., 2020b) and the RDP classifier (Wang et al., 2007), implemented with DADA2. This release was supplemented with full ITS sequences belonging to fungal taxa known to associate with *P. menziesii* or other conifers, but not included in the UNITE release. The full ITS sequence of *P. menziesii* was also included in the release, allowing for host amplification to be identified and removed. The PERFect R package was used to remove spurious OTUs by identifying those OTUs which made insignificant contributions to the total covariance of the dataset (Smirnova et al., 2019); the permutation method with default significance thresholds (retaining OTUS with $P < 0.1$, with P values calculated using 1000 permutations) was applied. Altogether, LULU conditional OTU curation and PERFect filtering were employed as a means to retain as much sequence resolution as possible while also attempting to minimize the effects of infragenomic taxon splitting and artifactual sequence generation.

2.3. Airborne LiDAR data-processing

Crown closure values associated with each sample height were obtained by processing light detection and ranging point cloud data that had been collected for a larger survey of the McKenzie River study area. Between June 07, 2016 and June 21, 2016, Quantum Spatial (Portland, Oregon, now NV5 Geospatial, Hollywood, Florida, USA), commissioned by the Oregon LiDAR Consortium, obtained discrete-return airborne laser scans of the HJA area from a Leica ALS80 (Leica Geosystems, St. Gallen, Switzerland) mounted on a Cessna Grand Caravan (Textron Aviation Inc., Wichita, Kansas, USA), flying 1500 m above ground level. Across the entire 2016 McKenzie River survey area, an average pulse density of 12.64 m^{-2} (SD = 4.867, min = 6.70 pulses m^{-2}, max = 65.66 pulses m^{-2}) was verified by the Oregon Department of Geology and Mineral Industries. Using 1,723 ground survey points, it was also found that the aerial survey had a horizontal accuracy of 0.37 m root mean square error (RMSE) and a vertical accuracy of 0.053 m RMSE. Point cloud data from this survey (OCM Partners, 2020) were downloaded from the NOAA Data Access Viewer as a projection to UTM Zone 10 (horizontal datum = NAD83 (2011), vertical datum = NAVD88, geoid = GEOID18), with meters as horizontal and vertical units.

Point clouds were processed with the lidR package (Roussel et al., 2020). Point clouds were purged of point returns with GPS time errors and intensity values of zero. For each tree, cylindrical volumes with radius 10 m (and centered on tree positions) were clipped from these

point clouds. This was the minimum radius that contained the horizontal breadth of each crown for each sampled tree. Prior to clipping, tree positions were refined, starting with GPS coordinates on record for each tree. The expertise of the HJA forest director (Dr. Mark Schulze) was used to verify final tree positions, which were centered on each treetop. For each cylinder containing the point cloud of each tree, the bare earth elevation under each tree was estimated via k-nearest neighbor inverse-distance weighting (k-nearest neighbor points = 10) using all available ground points. This bare earth elevation was added to the heights at which needle material was sampled in each tree. From here, a crown closure index was defined for each sampled tree height as the number of point returns above the sampled height, divided by the total number of point returns in each cylinder (Lovell et al., 2003). These closure values were then multiplied by the median height of elevation-normalized, non-ground point returns (Z_{med}, Fig. 1C) to account for the fact that a point cloud cylinder with a greater amount of tall vegetation will generally yield more, intervening point returns than a cylinder containing shorter vegetation (assuming equal scan coverage).

2.4. Analysis

To determine how needle community composition varied across trees, needle ages, and crown properties, features for each sample were relativized by sample sequencing depth (i.e., converted to relative abundance), and a generalized log transformation was applied to dampen the compositional influence of highly abundant OTUs. Bray-Curtis dissimilarity matrices were generated for use in downstream analyses. All subsequent analyses and ordinations were performed using functions from the vegan R package (Oksanen et al., 2020) unless stated otherwise. Dissimilarities associated with the full dataset were ordinated with non-metric multidimensional scalings (NMDS), using a two-dimensional solution. NMDS significance was evaluated by performing a Monte Carlo test (with 999 permutations) on the results using R scripts (calling vegan functions) modified from those originally created by Dr. Kevin McGarigal (pers. comm.). Four samples which prevented the NMDS ordination from converging were purged from the first needle age class. In trimming each needle age subset down to only the samples that shared a tree height with every other subset prior to analysis, samples were removed from the other three needle age classes if one needle age class was missing. This resulted in the retention of 64 samples for each needle age class subset (256 samples total). Permutation analyses of variance (PERMANOVA; Anderson, 2001) were performed with the *adonis2* function on the full dataset to determine whether needle compositions differed by tree and needle age, and the homogeneity of variances among levels of each factor was tested using the *betadisper* (implementing PERMDISP2; Anderson, 2006) and *permutest* functions to assess whether differences in composition were influenced by differences in group dispersion. For these tests, 999 random permutations were used to generate null pseudo-F ratio distributions, designating source tree ("tree") as a permutation stratum. Analyses were then followed by a PERMANOVA on the full dataset testing the effects of height and closure after accounting for needle age class, employing 999 permutations to generate P values and with "tree" as permutation stratum. Distance-based redundancy analyses (dbRDA) were constrained on crown variables, and PERMANOVAs were performed on each needle age subset to determine whether compositional variation accounted for by both crown variables changed with each needle age class.

Crown terms (i.e., among height and closure) accounting for unique compositional variation in the marginal test on the full dataset were retained to generate exposure groups. To ensure that group assignment procedure was not influenced by the small sampling of trees in our dataset, the point clouds of 5828 randomly sampled trees across HJA were also characterized by calculating closure at 10 random heights in each tree, using the method described above (Fig. 1B). Random sampling was restricted to trees attaining the minimum treetop height (35 m) and Z_{med} (22.67 m) values observed among the climbed trees in our dataset, and random height sampling was also restricted to the range observed for climbed trees (lowest height = 10 m, greatest height = 55 m). Closure values calculated at each sampled height were clustered into two groups using the Hartigan-Wong k-means clustering algorithm (Hartigan and Wong, 1979) with the maximum number of iterations and the number of random starts both set to 999. Samples from heights associated with the lower mean cluster were designated as belonging to the "open" exposure group, and samples associated with the higher mean cluster were designated as belonging to the "closed" exposure group. This was followed by indicator species analysis on the full dataset (Dufrene and Legendre, 1998; as implemented with the labdsv package by Roberts, 2019), which was used to identify taxa that occurred more frequently and with greater relative abundance than expected by chance in either open or closed exposure groups. Only OTUs occurring in at least 10% of samples were subjected to indicator species analysis. P-values were adjusted to control for the false discovery rate of indicator taxa using a Benjamini-Hochberg correction (Benjamini and Hochberg, 1995).

To determine whether alpha diversity varied with tree, needle age, and closure, and height richness (Hill number $q = 0$) and the exponent of Shannon entropy ($q = 1$) were estimated for each sample using the iNEXT package (Hsieh et al., 2016). Both metrics were estimated at a depth of 1000 reads, and variation in richness and $\log_2$-transformed Shannon entropy (i.e, the Shannon index of diversity) was tested among source tree and needle age (and their interaction) using analysis of variance (ANOVA) *F*-tests (Fox and Weisberg 2019). Assumptions of normality and homoscedasticity were investigated. In the event of putative heteroscedasticity, a White standard error adjustment was applied in an attempt to correct for its influence in the ANOVA (Long and Ervin, 2000). Results of F-tests were investigated further with Tukey honest significant differences *post-hoc* tests (alpha = 0.05). Alpha diversity means were bootstrapped and confidence intervals were generated with the *bca* function of the coxed R package (Kropko and Harden, 2020). Linear mixed-effect models were created using the nlme package (Pinheiro et al., 2021) to test the correlations of alpha diversity metrics with closure and height, setting source tree as a random effect. Reduced models containing either height or closure were compared to each other, a full model containing both crown variables, and a base model that only contained the tree random effect according to their corrected Akaike information criterion (AICc) and Bayesian information criterion (BIC) values using the AICcmodavg R package (Mazerolle, 2020). Reduced model P-values were obtained by performing a likelihood-ratio test comparing the reduced model to the base model. Models included needle age class as a fixed effect term if the term was significant in earlier ANOVAs. Pseudo-R^2 values of fixed effects were calculated using the piecewiseSEM package (Lefcheck, 2016).

Open and closed exposure groups were examined for changes in community structure over time by performing Mantel tests at each transition between needle age classes (A1 to A2, A2 to A3, A3 to A4). Rows and columns associated with samples belonging to either the open or closed exposure groups were extracted from the Bray-Curtis distance matrix associated with each needle age class and used as input matrices for Mantel tests, each using 999 permutations, setting source tree as a permutation stratum. Spearman ranked Mantel statistics were also bootstrapped with 999 permutations. With each permutation, tree heights shared by the needle age classes being compared were randomly sampled with replacement and the Bray-Curtis dissimilarity matrix was generated among the corresponding samples belonging to each needle age class. As above, samples belonging to either the open or closed exposure groups were extracted and the ranked Spearman correlation between matrices was found. Means were calculated from these bootstrapped correlation coefficients, and confidence intervals were generated as above. To compare the relative abundances of dominant OTUs across needle age transitions, paired Wilcoxon signed rank tests were

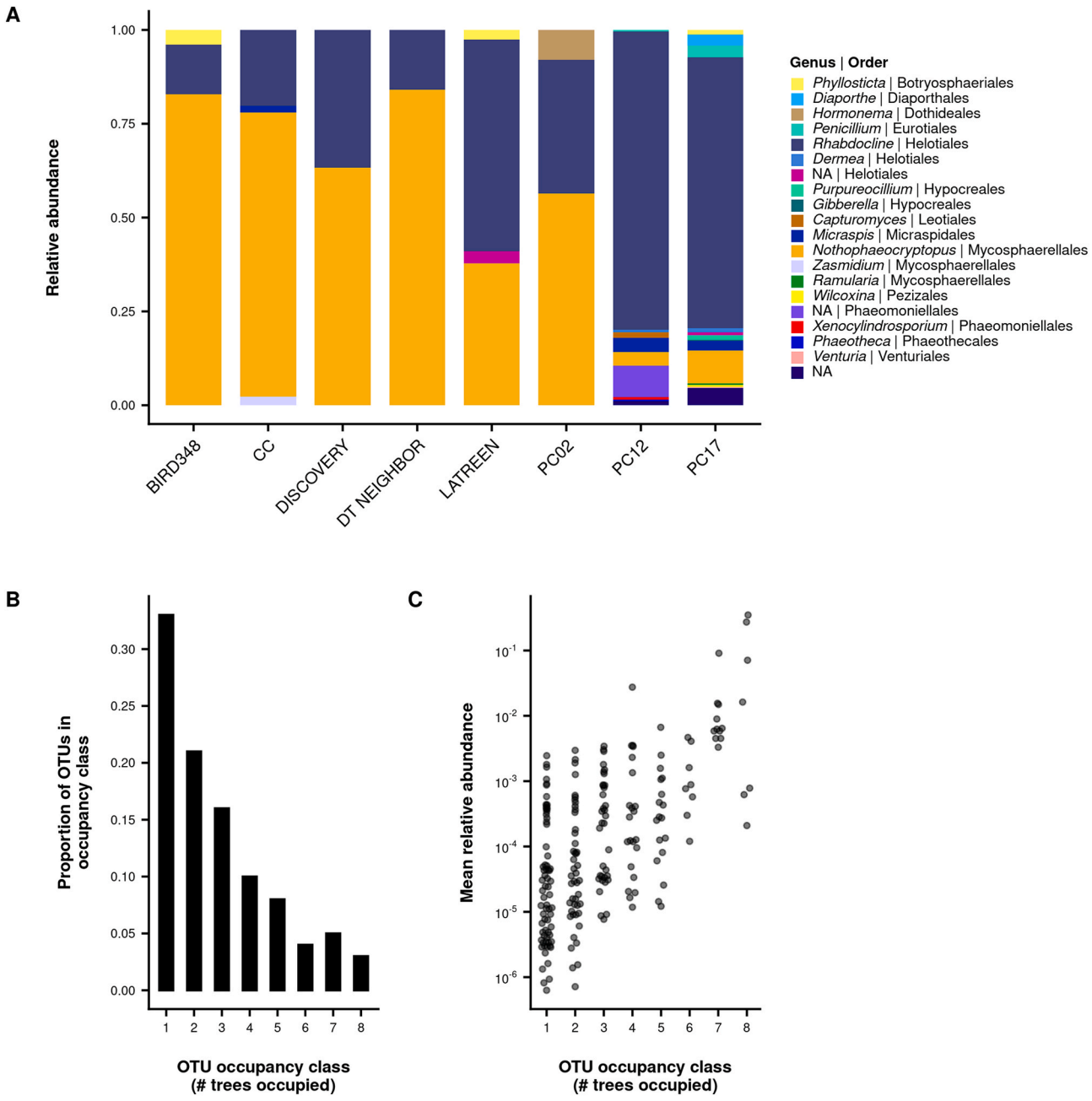

Fig. 2. Taxonomic assignments of OTUs present in the top 95% of reads, pooled at the tree-level (A). OTUs are colored by genus. OTU abundance distribution across the eight trees sampled in this study (B). Occupancy-abundance curve, plotting the mean relative abundance of each OTU against the number of trees it was found to occupy (C). The y-axis of (C) was log10-transformed. Each point represents a different OTU.

performed in R. When the null hypothesis was rejected for a pair of age classes (alpha = 0.05), a two-sample Wilcoxon ranked sum test was performed comparing OTU relative abundances between open and closed exposure groups for the older needle age class. Exact P values (as opposed to normally approximated P values) were calculated when possible.

2.5. Reproducibility

All statistical analyses were conducted in the R v4.0.3 statistical computing environment (R Core Team 2020). The functions associated with the tidyverse R package (Wickham et al., 2019) featured heavily in many scripts and facilitated the manipulation of data structures. Handling of metabarcoding data was accomplished with the phyloseq package (McMurdie and Holmes, 2013). Novel code and metadata associated with bioinformatics, point cloud processing, statistical analyses, and figures have been publicly archived (https://doi.org/10.5281/zenodo.6360767). Demultiplexed sequencing data are deposited in the NCBI Sequence Read Archive (BioProject ID PRJNA748821, BioSample accession SAMN20345134). LiDAR point cloud data are available for download from the NOAA data portal (https://www.fisheries.noaa.gov/inport/item/49949).

3. Results

3.1. Overview

Before the removal of contaminants and non-fungal sequences, ITS

Table 1
PERMANOVA results displaying the amount of compositional variation accounted for by needle age and tree, and the marginal variation of height and crown closure. P values are the results of permutation tests of pseudo F-ratios using 999 iterations, setting "tree" as a stratum.

	Df	R^2	F	P
Age class and tree				
Tree	7	0.266	14.568	0.001
Age	3	0.059	7.537	0.001
tree:age	21	0.090	1.636	0.001
Residual	224	0.585		
Total	255	1.000		
Age class and crown variables				
age:height	4	0.023	1.654	0.124
age:closure	4	0.053	3.753	0.001
Residual	244	0.859		
Total	255			

extraction, chimera removal, and LULU clustering, 1786 ASVs were identified across 284 non-control samples. After ITS extraction, there were 1316 ASVs and 1292 ASVs after chimera filtering. 138 ASVs were attributed to *Pseudotsuga* ITS sequences, totalling 561,671 reads. 1115 putatively fungal ASVs were retained after the VSEARCH filtering process. After 97% LULU clustering and contaminant removal, 899 OTUs were delineated, represented by 6,123,130 sequences over 282 samples. This was reduced to 218 OTUs, 5,001,904 sequences, and 256 samples after PERFect OTU filtering, contaminant removal, and the removal of samples that did form a full complement of needle age classes. OTU accumulation curves, generated with functions from the BiodiversityR package (Kindt and Coe 2005), indicated that each tree was adequately sampled (Fig. S1).

3.2. Composition

OTU.1, identified as *Nothophaeocryptopus gaeumannii* (Mycosphaerellales, Dothideomycetes), was the most dominant OTU in the dataset, followed by OTUs identified as *Rhabdocline parkeri* (OTU.2, OTU.3, and OTU.6; Helotiales, Leotiomycetes) (Fig. 2A). 54% of the OTUs retained occurred on two or fewer trees, while only 3% of OTUs occurred on every tree (Fig. 2B). Only eight of 218 OTUs (3.67%) achieved average relative abundances greater than 1%, with *Penicillium expansum* (OTU.65) representing the lower end of this subset (1.5%, Fig. 2C). Analyzing the full dataset revealed that source tree ($F = 14.568$, $P = 0.001$, $R^2 = 0.266$) and needle age class ($F = 7.537$, $P = 0.001$, $R^2 = 0.059$) accounted for a large portion of variation in community composition (Table 1; Fig. S2). However, these differences were influenced by unequal variance among levels within each factor ($7.643 < F < 11.575$, $P = 0.001$, Table S1). Marginal testing revealed that only crown closure accounted for unique components of variation ($F = 3.753$, $P = 0.001$, $R^2 = 0.053$; Table 1). This proportion increased when untransformed relative abundance data were used ($F = 6.294$, $P = 0.004$, $R^2 = 0.085$). When performing PERMANOVAs on each needle age subset individually, crown closure accounted for the most compositional variation in needle age classes A2 ($F = 5.849$, $P = 0.001$, $R^2 = 0.084$) and A3 ($F = 4.637$, $P = 0.002$, $R^2 = 0.068$; Table S2, Fig. 3B and Fig. 3C).

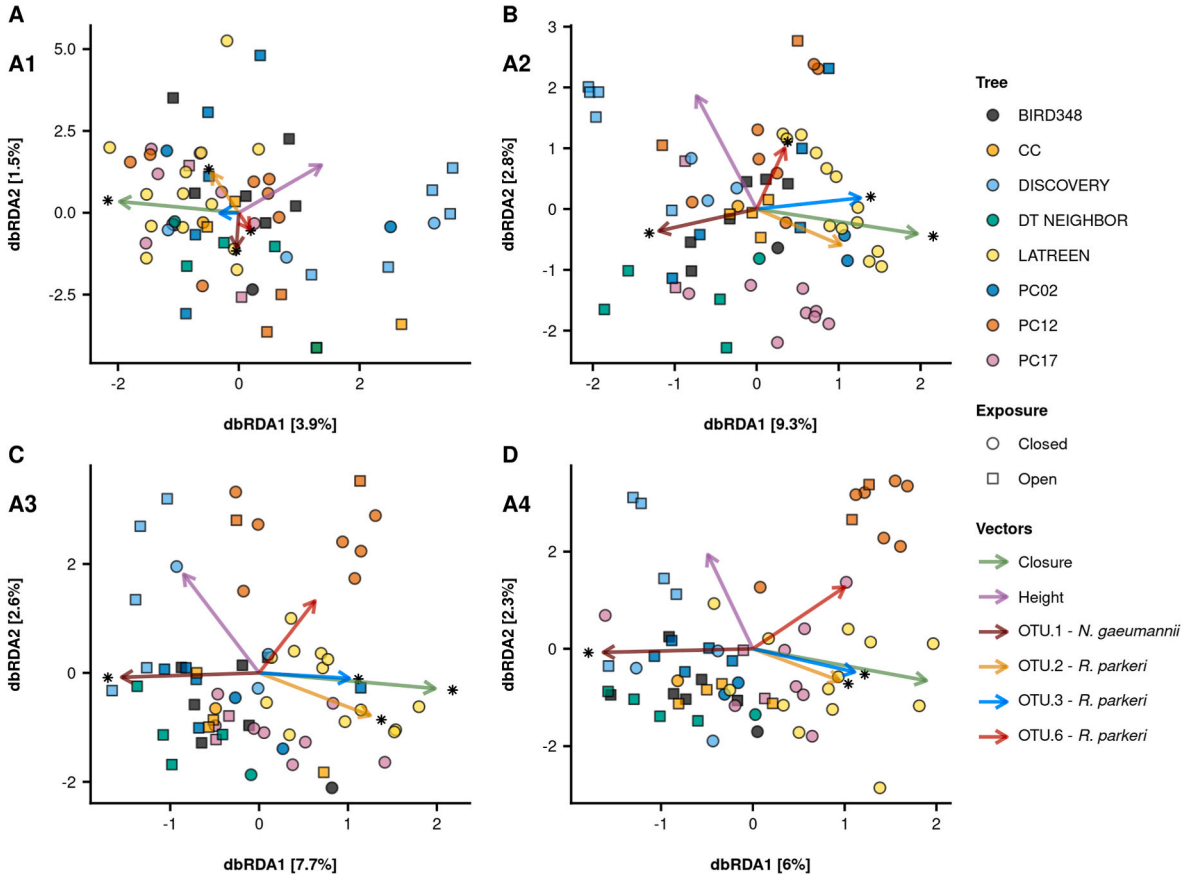

Fig. 3. Distance-based redundancy analyses (dbRDA) of Bray-Curtis dissimilarities for each needle age subset, constrained on height and crown closure. OTU vectors demonstrate correlations between ordination axes and untransformed OTU relative abundances, as assessed with the *envfit* function from the vegan R package, while crown variable vectors are extracted directly from the dbRDA biplot scores. Asterisks are associated with significant vectors (alpha = 0.05), longer vectors signify stronger correlations, but vector length should only be compared within crown variable and OTU vectors. Vector significance was assessed with 999 permutations, treating "tree" as a permutation stratum; tests involving crown variables were marginal pseudo-F tests.

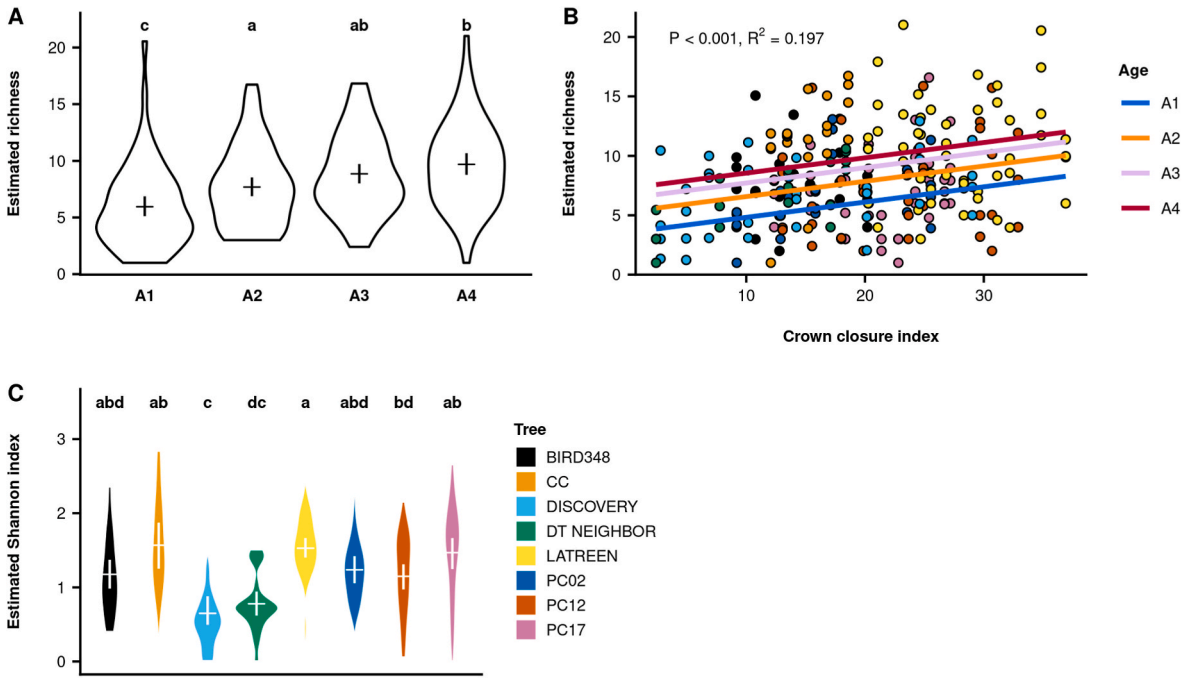

Fig. 4. Estimates of OTU richness or the Shannon index of diversity associated with needle age (A), crown closure index (B), and tree (C). Estimates were obtained for each sample via interpolation or extrapolation to a depth of 1000 reads. Violin plots illustrate the distribution of richness and Shannon index diversity estimates for each grouping. Letters for (A) and (C) indicate significant difference groups from Tukey HSD *post-hoc* comparisons (alpha = 0.05) among levels of each factor after performing ANOVA F-tests. Horizontal lines delineate the bootstrapped means of estimates, while vertical lines correspond to bootstrapped 95% confidence intervals (n = 999).

When this same analysis was performed with untransformed relative abundance data, closure only accounted for a significant component of variation in needle age class A3 ($F = 9.679$, $P = 0.003$, $R^2 = 0.131$). Given these results, only crown closure was used to define exposure groups. Exposure group assignment resulted in relatively similar numbers of open (n = 28) and closed (n = 36) exposures. Across all trees and needle age classes, OTU.1 (estimated as *N. gaeumanni*) was found to strongly associate with needles in open exposures ($P = 0.006$, IV = 0.629) and OTU.2 (*Rhabdocline parkeri*) was the strongest indicator taxon for closed exposures ($P = 0.009$, IV = 0.488). Another *Rhabocline parkeri* OTU (OTU.3) was also identified as an indicator taxon for closed exposures ($P = 0.022$, IV = 0.482). The roster of closed exposure indicator taxa exceeded the roster of open exposure indicators (Table S3).

3.3. Diversity

OTU richness varied across trees ($F = 11.264$, $P < 0.001$) and needle ages ($F = 16.343$, $P < 0.001$), increasing with needle age class (Fig. 4A) and with increasing crown closure ($\Delta AICc_{min} = 1.97$, AICc weight = 0.67, $\Delta BIC_{min} = 4.31$, BIC weight = 0.84, $P < 0.001$, $R^2 = 0.197$; Fig. 4B). Additionally, the Shannon index of diversity varied among trees ($F = 32.209$, $P < 0.001$; Fig. 4C). The Shannon index of diversity was also found to increase with increasing closure ($\Delta AICc_{min} = 1.06$, AICc weight = 0.50, $\Delta BIC_{min} = 1.06$, BIC weight = 0.60, $P < 0.001$, $R^2 = 0.079$; Fig. S3).

3.4. Structure

Fungal community composition from heights in the open and closed exposure groups were differentially structured over needle age class transitions (Fig. 5). For closed exposures, community structure became increasingly correlated over the A1-A4 transitions. No significant structural correlation was detected at the A1 to A2 transition ($P = 0.762$), nor for the A2 to A3 transition ($P = 0.204$) but community structures were strongly correlated with each other at the A3 to A4 ($P = 0.034$, Spearman correlation $\rho = 0.782$). Conversely, the community structures of open exposures were not correlated at any transition stage ($P \geq 0.220$). The relative abundance of *N. gaeumannii* (OTU.1) in all exposures only increased at the A2 to A3 transition (Wilcoxon signed rank test, $V = 208$, $P < 0.001$). OTU.1 relative abundances in closed exposures, however, remained lower than relative abundances in open exposures at A3 (Wilcoxon rank sum test, $W = 815.5$, $P < 0.001$) with slightly elevated proportions in A3 and A4 (Fig. 6A). Conversely, *R. parkeri* OTUs (OTU.2, OTU.3, and OTU.6) across all exposures increased in relative abundance from A1 to A2 ($V = 406$, $P < 0.001$), but larger relative abundances were achieved in closed exposures at A2 ($W = 238$, $P < 0.001$, Fig. 6B). These *R. parkeri* OTUs decreased in relative abundance at the A2 to A3 transition ($V = 1649$, $P < 0.001$), but closed exposures had higher relative abundances than open exposures ($W = 206$, $P < 0.001$) at A3.

4. Discussion

This study is the first of its kind to combine airborne LiDAR-derived metrics with fine-scale, within-crown foliage sampling of known needle age classes, and high-throughput amplicon sequencing. Additionally, forest-level LiDAR data were exploited to more objectively classify the crowns of climbed trees in the dataset. Altogether, these approaches showed that the diversity, composition, and structure of the endophytic needle mycobiome are correlated with the surrounding crown microenvironment in a way that depends on the age classes of needles. This study demonstrates the unique utility that remote sensing technologies like LiDAR can provide to studies of "hard-to-reach" ecological communities, while also allowing researchers to frame the sometimes limited environmental variation among their sampled sites in the context of variation observed at larger scales. Further, the high throughput amplicon sequencing approach taken here resulted in identifications of the same dominant taxa described in earlier, established work. Namely, *Nothophaecryptopus gaeumannii* (Stone et al., 2008), *Rhabdocline parkeri* (Sherwood-Pike et al., 1986), and *Phyllosticta*

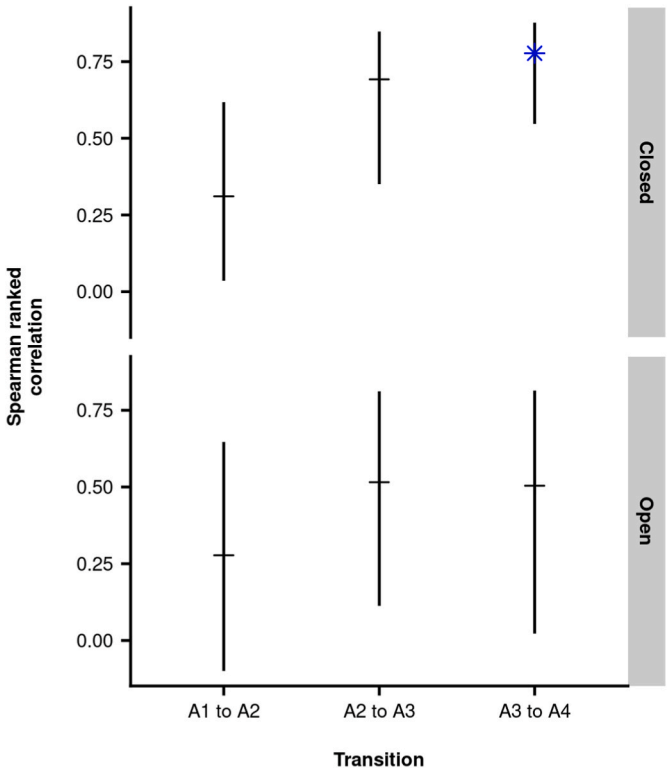

Fig. 5. Spearman Mantel correlations between increasing needle age classes for samples in open and closed exposure groups. Horizontal lines show the mean bootstrapped correlation statistics (n = 999), and vertical lines show the bootstrapped 95% confidence intervals. Higher correlation statistics indicate greater similarities in community structure between two needle age classes. Results of sample estimate Mantel tests with P < 0.05 are indicated by blue asterisks. P values were the result of 999 permutations, treating "tree" as permutation stratum.

spp. (Petrini et al., 1991) have been described as key members of the *Pseudotsuga menziesii* needle endophyte community. Taxa previously reported on the *P. menziesii* phylloplane or spermosphere (or associated with other conifers) were also frequently detected. These included *Zasmidium pseudotsugae* (Barr, 2009), *Hormonema macrosporum* (Bergmann and Busby, 2021), *Diaporthe* spp. (Gomes et al., 2013), *Micraspis strobilina* (Quijada et al., 2020), Phaeomoniellaceae sp. (Chen et al., 2015, Fig. 2).

4.1. Crown closure, interacting with needle age, accounted for more community variation than height

Source tree accounted for the greatest amount of compositional variation among samples (Table 1, Fig. S2), likely due to the large number of OTUs specific to only one or a few trees (Fig. 2). These results are similar to those of Harrison et al., (2016) and Oono et al., (2017), where, despite spatial ranges differing between the three studies by an order of magnitude (~10 km for the current study vs ~100 km for Oono et al. vs ~700 km for Harrison et al.), source tree or site also accounted for a large portion of variation in the composition of the foliar endophytic mycobiome of conifers. Further, these and other (Izuno et al., 2016), earlier studies find compositional differences between sampled crown positions. Analogous to crown position, height measured in the present study was unable to account for unique compositional variation (Table 1), perhaps suggesting that previously reported vertical stratification effects are actually unmeasured crown closure effects, given that crown closure decreases monotonically with increasing height in crown. This is supported by culture-based and visual survey studies which showed that certain foliar fungal taxa appeared to demonstrate preferences for either qualitatively defined shaded or exposed foliage (Osono and Mori, 2004; Gilbert et al., 2007; Unterseher et al., 2007; Scholtysik et al., 2013), but this effect is not consistently observed (Taudière et al., 2018). However, other work examining terrestrial macrofungal communities has established correlations between airborne LiDAR-derived measurements of canopy cover, maximum canopy height aboveground, and compositional turnover (Thers et al., 2017). In any case, quantifying exposure beyond canopy position or height should facilitate comparisons between studies of crown-associated foliar fungi (Arnold and Herre, 2003).

Analyzing each needle age class separately showed that compositional signal attributable to crown closure was detected at all needle ages, but peaked at A2 and A3 (Table S2, Fig. 3). The closure signal was stronger overall, but constrained to one needle age class when metabarcoding data were analyzed according to relative abundances that were not log-transformed. This result is indicative of the extent to which endophytic fungal communities were dominated by a few common taxa, a condition also reported by Harrison et al., (2016). Regardless of whether rarer or more common taxa were given more weight, closure-mediated compositional signal continued to collapse after needle age class A3 (Fig. 3). Thus, this shift in community composition for older needle age classes marks when smaller-scale, intra-crown community dynamics might give way to larger-scale or non-closure-mediated assembly dynamics. Needle age class has also been found to account for compositional variation of foliar fungal communities in both metabarcoding (Würth et al., 2019) and culture-based studies (Osono, 2008), and this is likely due to higher incidences of infection observed for older needle age classes (Sherwood and Carroll, 1974; Bernstein and Carroll, 1977; Petrini and Carroll, 1981) resulting from longer exposure to inoculum sources (Arnold and Herre, 2003). However, differences in needle physiology and morphology also accrue with increasing needle age class (Porte and Loustau, 1998; Bernier et al., 2001; Apple et al., 2002; Ishii et al., 2002; Yan et al., 2012; Eimil-Fraga et al., 2015), potentially accounting for its influence on endophyte community composition.

The relevance of crown closure is also supported by the finding that OTU richness and diversity increased with increasing closure (Fig. 4B, Fig. S3), with the model selection process explicitly excluding height. Again, these findings are similar to those reported from foliar fungal surveys and airborne LiDAR-supported macrofungal studies (Osono and Mori, 2004; Gilbert et al., 2007; Unterseher et al., 2007; Scholtysik et al., 2013; Thers et al., 2017), but evidence from metabarcoding studies is mixed and complicated by the inconsistent use of canopy position or light exposure groups between studies (Harrison et al., 2016; Izuno et al., 2016; Oono et al., 2017; Taudière et al., 2018). If compared with findings that composition and richness vary along larger-scale temperature and precipitation gradients (Giauque and Hawkes, 2016; Bowman and Arnold, 2021; Oita et al., 2021), the results observed in the current study might suggest the more immediate action of microclimate-mediated environmental filtering mechanisms that operate at smaller scales. However, this interpretation relies on the strength of the relationship between within-crown LiDAR and microclimatic metrics, which has yet to be sufficiently demonstrated. Further, physiological and morphological needle traits vary within the crowns of conifers in response to these same microclimatic gradients (Ishii et al., 2002, 2008; Gebauer et al., 2015; Schweiger et al., 2020), and this variation may have the potential to act with even more immediacy in structuring conifer endophyte communities. In fact, correlations of crown closure with composition and diversity can still suggest a role for closure-mediated dispersal limitation in structuring these communities (Gilbert and Reynolds, 2005), modifying the effect of closure-mediated environmental filtering.

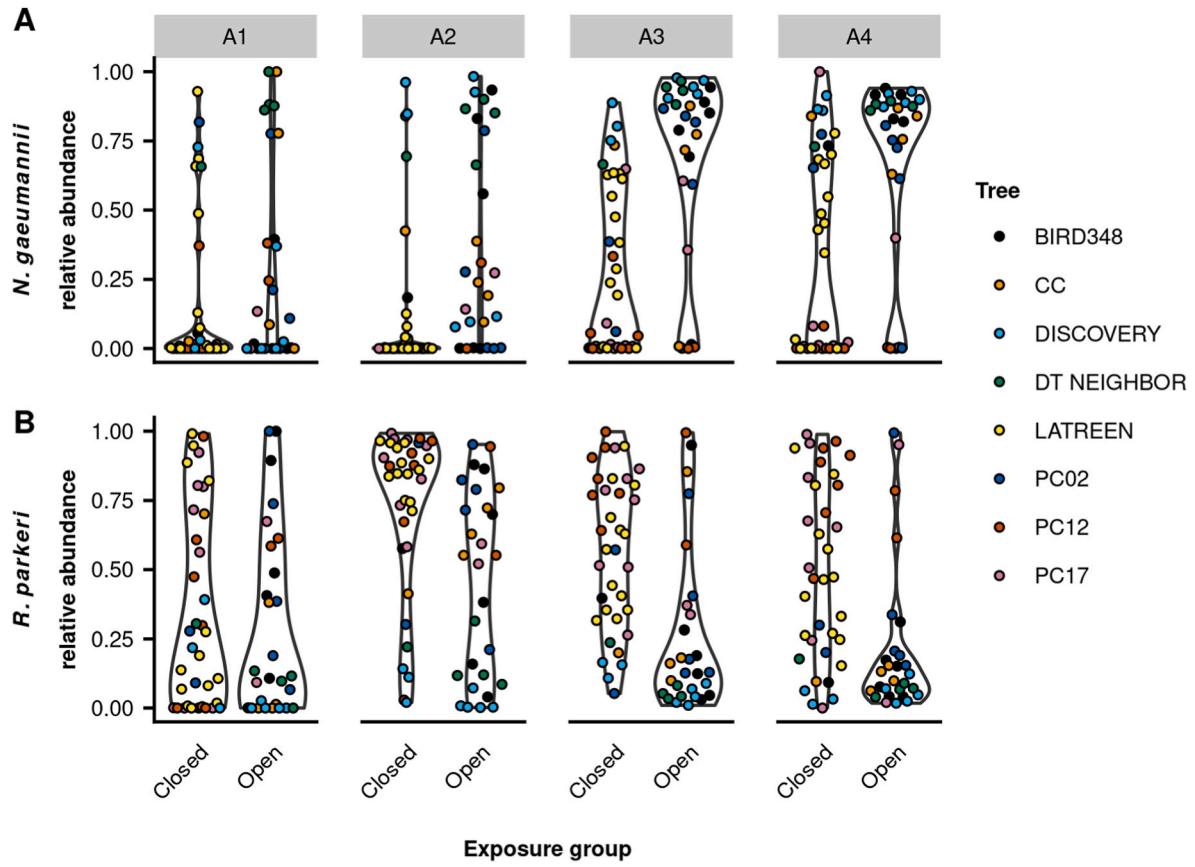

Fig. 6. Relative abundances of OTU.1 (identified to *Nothophaeocryptopus gaeumannii*) (A) and OTU.2, OTU.3, and OTU.6 (identified to *Rhabdocline parkeri*) (B) in each exposure group and needle age class.

4.2. Community structure diverges via interactions between needle age and needle exposure

Further exploration of needle age class and exposure group showed that inter-age differences in community structure differed between open and closed exposure groups. Although no structural correlations were detected at the A1-A2 and A2-A3 transitions for both exposure groups, strongly correlated structure was detected for closed exposures at the A3-A4 transition, indicating that turnover proceeded in a way that preserved some of the structure associated with the previous needle age class (Fig. 5). Conversely, open exposures never demonstrated significant structural correlations, signifying dynamic shifts in one or many compositional elements between needle age classes. Although the relative abundance of open exposure indicator OTU.1 (identified as *Nothophaeocryptopus gaeumannii;* Table S3) increased at the A2 to A3 transition, this increase was less pronounced for needles sampled from closed exposures (Figs. 3 and 6A), suggestive of altered community assembly dynamics relative to needles from open exposures. However, without sampling even older needle age classes, it is not apparent that (1) endophyte communities in needles from closed exposures would ever fully converge on a composition defined by *N. gaeumannii* dominance, (2) that the community structure of needles from open exposures ever stabilizes, or (3) that closed exposures retain age-class-to-age-class community structure.

Overall, observations from this study align with what is known about the infection cycle of *N. gaeumannii* and the general pathology of the Swiss needle cast (SNC) disease it can cause in *P. menziesii*. Conidium production has never been observed. Instead, needles are initially infected solely via ascospores (Stone et al., 2008) dispersed by rain. Ascospore release generally coincides with *P. menziesii* bud burst, and older needles appear to resist ascospore infection to some degree, leading pathologists to conclude that infection primarily occurs on newly emerged foliage during the spring and summer. After entering via stomata, *N. gaeumannii* proceeds to extensively colonize intercellular spaces over the lifetime of the needle, perhaps assisted by periodic epiphytic growth and stomatal reentry. Thus, continued colonization after early infection likely accounted for the majority of the observed increases in *N. gaeumannii* relative abundance at each needle age class transition (Fig. 6). The extent of this advantage was apparent given that the increase in OTU richness from A1 to A4 (Fig. 4A) was not met with an increase in the Shannon index of diversity over these needle age classes (Table S4). This suggests that while other taxa are able to at least infect a needle over its lifetime, they are generally unable to colonize the needle as effectively as *N. gaeumannii* over this period. The greater relative abundance and incidence of *N. gaeumannii* OTU.1 in open exposures is corroborated by experimental findings that shade-treated *P. menziesii* seedlings showed reduced SNC severity relative to the full-sun treatments (Manter et al., 2005). This measure of severity was also correlated with higher winter temperatures measured over the course of the experiment. Results from this earlier experiment are also in accordance with the common observation that SNC disease severity is negatively correlated with depth in crown in natural and managed stands of *P. menziesii* (Hansen et al., 2000; Lan et al., 2019, 2022; Ritokova et al., 2020). A greater abundance of *N. gaeumannii* in warm, open exposures could reflect morphological and/or physiological adaptations to this niche. For example, previous work has reported that cultures of *N. gaeumannii* can deposit red pigments into the growth medium, suggesting that *N. gaeumannii*, like *Cercospora* spp. also in the Mycosphaerellaceae, may produce cercosporin or cercosporin-like perylenequinones (Winton et al., 2007). Cercosporin, which is red in its active, oxidized state, was originally isolated from *Cercospora kikuchii* and since been shown to disrupt plant cell membranes via the

photoactivation of singlet oxygen (Daub and Ehrenshaft, 2000). Similar to SNC patterns, the incidence and progression of several diseases caused by perylenequinone-producing fungi (*Cercospora* spp., *Alternaria alternata*) are also positively associated with increased light exposure (Daub et al., 2013). Further investigation of the most recent assembly of the *N. gaeumannii* genome (BioProject PRJNA212511, BioSample SAMN02254965) with the antiSMASH BGC prediction program (fungiSMASH default parameters, Blin et al., 2021) revealed the presence of a putative cercosporin BGC resembling one found in *Cercospora beticola* with 31% similarity (Table S5). Additionally, a T1PKS melanin BGC was identified, showing 100% similarity with a cluster found in *Bipolaris oryzae*. These findings, taken alongside increasing relative abundance of *N. gaeumannii* with decreasing crown closure, suggest that *N. gaeumannii* may be adapted to a niche characterized by warm temperatures and/or pronounced light exposure.

In contrast to *N. gaeumannii*, dominant *Rhabdocline parkeri* OTUs (OTU.2, OTU.3) were identified as taxa associated with closed exposures (Table S3), which is also in accordance with the known biology of this endophyte. Conidia of *R. parkeri* infect needles of *P. menziesii* and remain within a single epidermal cell until the needle approaches senescence. Rain-dispersed conidia produced on abscised needles can infect living needles of all needle age classes during the wet winter months (Sherwood-Pike et al., 1986). Needles are soon overtaken by generalist saprotroph communities once abscised needles reach terrestrial leaf litter (Stone, 1987), but *R. parkeri* has been shown to dominate the endosphere of abscised needles shaken directly from ten year-old *P. menziesii* crowns (Gonen, 2020). These abscised needles lodged in the crown then serve as inoculum sources for new infections in the crown. To account for the results of our indicator species analysis, it is hypothesized that the crowns above closed exposures intercept and/or retain more abscised needles on branches compared to portions above open exposures. *P. menziesii* canopy soils are derived from bark and decomposing needles deposited on branches (Pike et al., 1975), and these soils might then serve as reservoirs for *R. parkeri* and potentially other endophytic fungi (Looby et al., 2020). The capacity for a tree crown to retain needle litter reservoirs close to living foliage might also be adaptive if fungi sourced from this litter can reduce pest or pathogen damage, as has been described for *R. parkeri* (Carroll, 1988). This reservoir effect could also account for the finding that OTU richness and diversity increased with increasing crown closure (Fig. 4B; Fig. S3). However, closed exposures could also be associated with more moist, thermostable, and otherwise accommodating microhabitats that are favorable to infection by *R. parkeri* and/or fungi in general, potentially accounting for or contributing to the indicator status of *R. parkeri* OTUs and the greater taxonomic diversity associated with closed exposures (Unterseher and Tal, 2006).

Declaration of competing interest

The authors declare no conflicts of interest.

Acknowledgements

Data were provided by the HJ Andrews Experimental Forest and Long Term Ecological Research (LTER) program, administered cooperatively by the USDA Forest Service Pacific Northwest Research Station, Oregon State University, and the Willamette National Forest. This material is based upon work supported by the National Science Foundation under LTER7 DEB-1440409 (2014–2020).

The authors would also like to acknowledge Dr. Mark Schulze, Dr. Adam Sibley, Robert Miron, and Sarah Ward for organizing and executing needle collection. Additionally, the authors thank the H.J. Andrews Forest Canopy Group for their interest and input throughout the execution and analysis of the study. Lastly, the authors also wish to recognize the significant contributions of Dr. George Carroll, Dr. Lawrence Pike, Dr. Martha Sherwood, and Dr. Jeffrey Stone to the study of *P. menziesii* crowns and needle fungi, which greatly facilitated interpretation of the results obtained here.

Appendix A. Supplementary data

Supplementary data to this article can be found online at https://doi.org/10.1016/j.funeco.2022.101155.

References

Abarenkov, K., Zirk, A., Piirmann, T., Pöhönen, R., Ivanov, F., Nilsson, R.H., Kõljalg, U., 2020a. UNITE general FASTA release for eukaryotes 2. Version 04.02.2020. UNITE Community. https://doi.org/10.15156/BIO/786371.

Abarenkov, K., Zirk, A., Piirmann, T., Pöhönen, R., Ivanov, F., Nilsson, R.H., Kõljalg, U., 2020b. UNITE general FASTA release for Fungi. Version 04.02.2020. UNITE Community. https://doi.org/10.15156/BIO/786368.

Anderson, M.J., 2001. A new method for non-parametric multivariate analysis of variance: non-parametric MANOVA for ecology. Austral Ecol 26, 32–46. https://doi.org/10.1111/j.1442-9993.2001.01070 x.

Anderson, M.J., 2006. Distance-based tests for homogeneity of multivariate dispersions. Biometrics 62, 245–253. https://doi.org/10.1111/j.1541-0420.2005.00440.x.

Apple, M., Tiekotter, K., Snow, M., Young, J., Soeldner, A., Phillips, D., Tingey, D., Bond, B.J., 2002. Needle anatomy changes with increasing tree age in Douglas-fir. Tree Physiol 22, 129–136. https://doi.org/10.1093/treephys/22.2-3.129.

Arnold, A.E., Engelbrecht, B.M.J., 2007. Fungal endophytes nearly double minimum leaf conductance in seedlings of a neotropical tree species. J. Trop. Ecol. 23, 369–372. https://doi.org/10.1017/S0266467407004038.

Arnold, A.E., Herre, E.A., 2003. Canopy cover and leaf age affect colonization by tropical fungal endophytes: ecological pattern and process in *Theobroma cacao* (Malvaceae). Mycologia 95, 388–398. https://doi.org/10.1080/15572536.2004.11833083.

Barge, E.G., Leopold, D.R., Peay, K.G., Newcombe, G., Busby, P.E., 2019. Differentiating spatial from environmental effects on foliar fungal communities of Populus trichocarpa. J. Biogeogr 46, 2001–2011. https://doi.org/10.1111/jbi.13641.

Barnes, K.W., Islam, K., Auer, S.A., 2016. Integrating LIDAR-derived canopy structure into cerulean warbler habitat models. J. Wildl. Manag. 80, 101–116. https://doi.org/10.1002/jwmg.995.

Barr, M.E., 2009. A nomenclator of loculoascomycetous fungi from the Pacific Northwest. North Am. Fungi 4, 1–94. https://doi.org/10.2509/naf2009.004.001.

Bengtsson-Palme, J., Ryberg, M., Hartmann, M., Branco, S., Wang, Z., Godhe, A., Wit, P. D., Sánchez-García, M., Ebersberger, I., de Sousa, F., Amend, A., Jumpponen, A., Unterseher, M., Kristiansson, E., Abarenkov, K., Bertrand, Y.J.K., Sanli, K., Eriksson, K.M., Vik, U., Veldre, V., Nilsson, R.H., 2013. Improved software detection and extraction of ITS1 and ITS2 from ribosomal ITS sequences of fungi and other eukaryotes for analysis of environmental sequencing data. Methods Ecol. Evol. 4, 914–919. https://doi.org/10.1111/2041-210X.12073.

Benjamini, Y., Hochberg, Y., 1995. Controlling the false discovery rate: a practical and powerful approach to multiple testing. J. R. Stat. Soc. Ser. B Methodol. 57, 289–300. https://doi.org/10.1111/j.2517-6161.1995.tb02031.x.

Bergmann, G.E., Busby, P.E., 2021. The core seed mycobiome of *Pseudotsuga menziesii* var. *menziesii* across provenances of the Pacific Northwest, USA. Mycologia, pp. 1–12. https://doi.org/10.1080/00275514.2021.1952830.

Bernier, P.Y., Raulier, F., Stenberg, P., Ung, C.-H., 2001. Importance of needle age and shoot structure on canopy net photosynthesis of balsam fir (*Abies balsamea*): a spatially inexplicit modeling analysis. Tree Physiol 21, 815–830. https://doi.org/10.1093/treephys/21.12-13.815.

Bernstein, M.E., Carroll, G.C., 1977. Internal fungi in old-growth Douglas fir foliage. Can. J. Bot. 55, 644–653. https://doi.org/10.1139/b77-079.

Blin, K., Shaw, S., Kloosterman, A.M., Charlop-Powers, Z., van Weezel, G.P., Medema, M. H., Weber, T., 2021. antiSMASH 6.0: improving cluster detection and comparison capabilities. Nucleic Acids Res 49, W29–W35. https://doi.org/10.1093/nar/gkab335.

Bowman, E.A., Arnold, A.E., 2021. Drivers and implications of distance decay differ for ectomycorrhizal and foliar endophytic fungi across an anciently fragmented landscape. ISME J 1–18. https://doi.org/10.1038/s41396-021-01006-9.

Busby, P.E., Peay, K.G., Newcombe, G., 2016. Common foliar fungi of *Populus trichocarpa* modify *Melampsora* rust disease severity. New Phytol 209, 1681–1692. https://doi.org/10.1111/nph.13742.

Callahan, B.J., McMurdie, P.J., Rosen, M.J., Han, A.W., Johnson, A.J.A., Holmes, S.P., 2016. DADA2: high-resolution sample inference from Illumina amplicon data. Nat. Methods 13, 581–583. https://doi.org/10.1038/nmeth.3869.

Carisse, O., Bourgeois, G., Duthie, J.A., 2000. Influence of temperature and leaf wetness duration on infection of strawberry leaves by *Mycosphaerella fragariae*. Phytopathology 90, 1120–1125. https://doi.org/10.1094/PHYTO.2000.90.10.1120.

Carroll, G., 1988. Fungal endophytes in stems and leaves: from latent pathogen to mutualistic symbiont. Ecology 69, 2–9. https://doi.org/10.2307/1943154.

Chen, K.-H., Miadlikowska, J., Molnár, K., Arnold, A.E., U'Ren, J.M., Gaya, E., Gueidan, C., Lutzoni, F., 2015. Phylogenetic analyses of eurotiomycetous endophytes reveal their close affinities to Chaetothyriales, Eurotiales, and a new order – Phaeomoniellales. Mol. Phylogenet. Evol. 85, 117–130. https://doi.org/10.1016/j.ympev.2015.01.008.

Christian, N., Herre, E.A., Clay, K., 2019. Foliar endophytic fungi alter patterns of nitrogen uptake and distribution in *Theobroma cacao*. New Phytol 222, 1573–1583. https://doi.org/10.1111/nph.15693.

Daub, M.E., Ehrenshaft, M., 2000. The photoactivated *Cercospora* toxin cercosporin: contributions to plant disease and fundamental biology. Annu. Rev. Phytopathol. 38, 461–490. https://doi.org/10.1146/annurev.phyto.38.1.461.

Daub, M.E., Herrero, S., Chung, K.-R., 2013. Reactive oxygen species in plant pathogenesis: the role of perylenequinone photosensitizers. Antioxidants & Redox Signaling 19, 970–989. https://www.liebertpub.com/doi/abs/10.1089/ars.2012.5080.

Davis, F.W., Synes, N.W., Fricker, G.A., McCullough, I.M., Serra-Diaz, J.M., Franklin, J., Flint, A.L., 2019. LiDAR-derived topography and forest structure predict fine-scale variation in daily surface temperatures in oak savanna and conifer forest landscapes. Agric. For. Meteorol. 269–270, 192–202. https://doi.org/10.1016/j.agrformet.2019.02.015.

Doughty, C.E., Goulden, M.L., 2008. Are tropical forests near a high temperature threshold? J. Geophys. Res. 113, G00B07. https://doi.org/10.1029/2007JG000632.

Eimil-Fraga, C., Sánchez-Rodríguez, F., Álvarez-Rodríguez, E., Rodríguez-Soalleiro, R., 2015. Relationships between needle traits, needle age and site and stand parameters in *Pinus pinaster*. Trees 29, 1103–1113. https://doi.org/10.1007/s00468-015-1190-7.

Fox, J., Weisberg, S., 2019. In: An R Companion to Applied Regression, third ed. https://doi.org/10.1126/sciadv.1501392 Thousand Oaks, California, USA.

Frey, S.J.K., Hadley, A.S., Johnson, S.L., Schulze, M., Jones, J.A., Betts, M.G., 2016. Spatial models reveal the microclimatic buffering capacity of old-growth forests. Sci. Adv. 2, e1501392 https://doi.org/10.1126/sciadv.1501392.

Frøslev, T.G., Kjøller, R., Bruun, H.H., Ejrnæs, R., Brunbjerg, A.K., Pietroni, C., Hansen, A. J., 2017. Algorithm for post-clustering curation of DNA amplicon data yields reliable biodiversity estimates. Nat. Commun. 8, 1188. https://doi.org/10.1038/s41467-017-01312-x.

Galanti, L., Shasha, D., C. Gunsalus, K., 2017. Pheniqs: fast and flexible quality-aware sequence demultiplexing. bioRxiv. https://doi.org/10.1101/128512.

Gebauer, R., Čermák, J., Plichta, R., Špinlerová, Z., Urban, J., Volařík, D., Ceulemans, R., 2015. Within-canopy variation in needle morphology and anatomy of vascular tissues in a sparse Scots pine forest. Trees 29, 1447–1457. https://doi.org/10.1007/s00468-015-1224-1.

George, A.D., Thompson, F.R., Faaborg, J., 2015. Using LiDAR and remote microclimate loggers to downscale near-surface air temperatures for site-level studies. Remote Sens. Lett. 6, 924–932. https://doi.org/10.1080/2150704X.2015.1088671.

Giauque, H., Hawkes, C.V., 2016. Historical and current climate drive spatial and temporal patterns in fungal endophyte diversity. Fungal Ecol 20, 108–114. https://doi.org/10.1016/j.funeco.2015.12.005.

Gilbert, G.S., Reynolds, D.R., 2005. Nocturnal fungi: airborne spores in the canopy and understory of a tropical rain forest. Biotropica 37, 462–464. https://doi.org/10.1111/j.1744-7429.2005.00061.x.

Gilbert, G.S., Reynolds, D.R., Bethancourt, A., 2007. The patchiness of epifoliar fungi in tropical forests: host range, host abundance, and environment. Ecology 88, 575–581. https://doi.org/10.1890/05-1170.

Gomes, R.R., Glienke, C., Videira, S.I.R., Lombard, L., Groenewald, J.Z., Crous, P.W., 2013. *Diaporthe*: a genus of endophytic, saprobic and plant pathogenic fungi. Persoonia Mol. Phylogeny Evol. Fungi 31, 1–41. https://doi.org/10.3767/003158513X666844.

Gonen, L., 2020. Community Ecology of Foliar Fungi and Oomycetes of *Pseudotsuga menziesii* on the Pacific Northwest Coast. Master's thesis. Oregon State University, Corvallis, Oregon, USA.

Hansen, E.M., Stone, J.K., Capitano, B.R., Rosso, P., Sutton, W., Winton, L., Kanaskie, A., McWilliams, M.G., 2000. Incidence and impact of Swiss needle cast in forest plantations of Douglas-fir in coastal Oregon. Plant Dis 84, 773–778. https://doi.org/10.1094/PDIS.2000.84.7.773.

Harrison, J.G., Forister, M.L., Parchman, T.L., Koch, G.W., 2016. Vertical stratification of the foliar fungal community in the world's tallest trees. Am. J. Bot. 103, 2087–2095. https://doi.org/10.3732/ajb.1600277.

Hartigan, J.A., Wong, M.A., 1979. Algorithm AS 136: a k-means clustering algorithm. Appl. Stat. 28, 100. https://doi.org/10.2307/2346830.

Heffernan, E., 2017. Canopy Microclimates and Epiphytes: Examining Dynamic Patterns and Influences. Master's thesis. Oregon State University, Corvallis, Oregon, USA.

Hsieh, T.C., Ma, K.H., Chao, A., 2016. iNEXT: an R package for rarefaction and extrapolation of species diversity (Hill numbers). Methods Ecol. Evol. 7, 1451–1456. https://doi.org/10.1111/2041-210X.12613.

Ishii, H., Ford, E.D., Boscolo, M.E., Manriquez, A.C., Wilson, M.E., Hinckley, T.M., 2002. Variation in specific needle area of old-growth Douglas-fir in relation to needle age, within-crown position and epicormic shoot production. Tree Physiol 22, 31–40. https://doi.org/10.1093/treephys/22.1.31.

Ishii, H.T., Jennings, G.M., Sillett, S.C., Koch, G.W., 2008. Hydrostatic constraints on morphological exploitation of light in tall Sequoia sempervirens trees. Oecologia 156, 751–763. https://doi.org/10.1007/s00442-008-1032-z.

Izuno, A., Kanzaki, M., Artchawakom, T., Wachrinrat, C., Isagi, Y., 2016. Vertical structure of phyllosphere fungal communities in a tropical forest in Thailand uncovered by high-throughput sequencing. PLOS ONE 11, e0166669. https://doi.org/10.1371/journal.pone.0166669.

Kindt, R., Coe, R., 2005. Tree Diversity Analysis. A Manual and Software for Common Statistical Methods for Ecological and Biodiversity Studies. World Agroforestry Centre.

Kropko, J., Harden, J.J., 2020. coxed: duration-based quantities of interest for the Cox proportional hazards model. R package version 0.3.3. https://doi.org/10.1002/ece3.1589.

Lan, Y.-H., Shaw, D.C., Beedlow, P.A., Lee, E.H., Waschmann, R.S., 2019. Severity of Swiss needle cast in young and mature Douglas-fir forests in western Oregon. USA. For. Ecol. Manag. 442, 79–95. https://doi.org/10.1016/j.foreco.2019.03.063.

Lan, Y.-H., Shaw, D.C., Lee, E.H., Beedlow, P.A., 2022. Distribution of a foliage disease fungus within canopies of mature Douglas-fir in Western Oregon. Front. For. Glob. Change 5, 743039. https://doi.org/10.3389/ffgc.2022.743039.

Lefcheck, J.S., 2016. piecewiseSEM: piecewise structural equation modelling in R for ecology, evolution, and systematics. Methods Ecol. Evol. 7, 573–579. https://doi.org/10.1111/2041-210X.12512.

Lefsky, M.A., Cohen, W.B., Parker, G.G., Harding, D.J., 2002. Lidar remote sensing for ecosystem studies: lidar, an emerging remote sensing technology that directly measures the three-dimensional distribution of plant canopies, can accurately estimate vegetation structural attributes and should be of particular interest to forest, landscape, and global ecologists. BioScience 52, 19–30. https://doi.org/10.1641/0006-3568(2002)052[0019:LRSFES]2.0.CO;2.

Long, J.S., Ervin, L.H., 2000. Using heteroscedasticity consistent standard errors in the Linear Regression Model. Am. Stat. 54, 217–224.

Looby, C.I., Hollenbeck, E.C., Treseder, K.K., 2020. Fungi in the canopy: how soil fungi and extracellular enzymes differ between canopy and ground soils. Ecosystems 23, 768–782. https://doi.org/10.1007/s10021-019-00439-w.

Lovell, J.L., Jupp, D.L.B., Culvenor, D.S., Coops, N.C., 2003. Using airborne and ground-based ranging lidar to measure canopy structure in Australian forests. Can. J. Remote Sens. 29, 607–622.

Manter, D.K., Reeser, P.W., Stone, J.K., 2005. A climate-based model for predicting geographic variation in Swiss needle cast severity in the Oregon Coast Range. Phytopathology 95, 1256–1265. https://doi.org/10.1094/PHYTO-95-1256.

Martin, M., 2011. Cutadapt removes adapter sequences from high-throughput sequencing reads. EMBnet.journal 17, 10–12. https://doi.org/10.14806/ej.17.1.200.

Mazerolle, M.J., 2020. AICcmodavg: model selection and multimodel inference based on (Q)AIC(c). R package version 2.3-1. https://cran.r-project.org/package=AICcmodavg.

McCune, B., 1993. Gradients in epiphyte biomass in three *Pseudotsuga-Tsuga* forests of different ages in western Oregon and Washington. The Bryologist 96, 405–411. https://doi.org/10.2307/3243870.

McMurdie, P.J., Holmes, S., 2013. phyloseq: an R package for reproducible interactive analysis and graphics of microbiome census data. PLoS ONE 8, e61217. https://doi.org/10.1371/journal.pone.0061217.

Norros, V., Karhu, E., Nordén, J., Vähätalo, A.V., Ovaskainen, O., 2015. Spore sensitivity to sunlight and freezing can restrict dispersal in wood-decay fungi. Ecol. Evol. 5, 3312–3326. https://doi.org/10.1002/ece3.1589.

Oita, S., Ibáñez, A., Lutzoni, F., Miadlikowska, J., Geml, J., Lewis, L.A., Hom, E.F.Y., Carbone, I., U'Ren, J.M., Arnold, A.E., 2021. Climate and seasonality drive the richness and composition of tropical fungal endophytes at a landscape scale. Commun. Biol. 4, 1–11. https://doi.org/10.1038/s42003-021-01826-7.

Oksanen, J., Blanchet, F.G., Friendly, M., Kindt, R., Legendre, P., McGlinn, D., Minchin, P.R., O'Hara, R.B., Simpson, G.L., Solymos, P., Stevens, M.H.H., Szoecs, E., Wagner, H., 2020. vegan: community ecology package. R package version 2.5-7. https://doi.org/10.2307/3242161.

Oono, R., Rasmussen, A., Lefèvre, E., 2017. Distance decay relationships in foliar fungal endophytes are driven by rare taxa: distance decay in fungal endophytes. Environ. Microbiol. 19, 2794–2805. https://doi.org/10.1111/1462-2920.13799.

Osono, T., 2008. Endophytic and epiphytic phyllosphere fungi of *Camellia japonica* : seasonal and leaf age-dependent variations. Mycologia 100, 387–391. https://doi.org/10.3852/07-110R1.

Osono, T., Mori, A., 2004. Distribution of phyllosphere fungi within the canopy of giant dogwood. Mycoscience 45, 161–168. https://doi.org/10.1007/S10267-003-0167-3.

Parker, G., 1997. Canopy structure and light environment of an old-growth Douglas-fir/western hemlock forest. Northwest Sci 71, 261–270.

Partners, O.C.M., 2020. 2016 Oregon department of Geology and mineral industries (DOGAMI) Oregon lidar: McKenzie river. https://www.fisheries.noaa.gov/inport/item/49949.

Petrini, O., Carroll, G., 1981. Endophytic fungi in foliage of some Cupressaceae in Oregon. Can. J. Bot. 59, 629–636. https://doi.org/10.1139/b81-089.

Petrini, L.E., Petrini, O., Leuchtmann, A., Carroll, G.C., 1991. Conifer inhabiting species of *Phyllosticta*. Sydowia 148–169.

Peura, M., Silveyra Gonzalez, R., Müller, J., Heurich, M., Vierling, L.A., Mönkkönen, M., Bässler, C., 2016. Mapping a 'cryptic kingdom': performance of lidar derived environmental variables in modelling the occurrence of forest fungi. Remote Sens. Environ. 186, 428–438. https://doi.org/10.1016/j.rse.2016.09.003.

Pike, L.H., Denison, W.C., Tracy, D.M., Sherwood, M.A., Rhoades, F.M., 1975. Floristic survey of epiphytic lichens and bryophytes growing on old-growth conifers in western Oregon. The Bryologist 78, 389–402. https://doi.org/10.2307/3242161.

Pinheiro, J., Bates, D., DebRoy, S., Sarkar, D., R Core Team, 2021. nlme: linear and nonlinear mixed effects models. R package version 3.1-152. https://CRAN.R-project.org/package=nlme.

Porte, A., Loustau, D., 1998. Variability of the photosynthetic characteristics of mature needles within the crown of a 25-year-old *Pinus pinaster*. Tree Physiol 18, 223–232. https://doi.org/10.1093/treephys/18.4.223.

Quijada, L., Tanney, J.B., Popov, E., Johnston, P.R., Pfister, D.H., 2020. Cones, needles and wood: *Micraspis* (Micraspidaceae, Micraspidales fam. et ord. nov.) speciation segregates by host plant tissues. Fungal Syst. Evol. 5, 99–111. https://doi.org/10.3114/fuse.2020.05.05.

R Core Team, 2020. R: A Language and Environment for Statistical Computing. R Foundation for Statistical Computing, Vienna, Austria. https://doi.org/10.1093/biostatistics/kxy020.

Ritokova, G., Mainwaring, D.B., Shaw, D.C., Lan, Y.-H., 2020. Douglas-fir foliage retention dynamics across a gradient of Swiss needle cast in coastal Oregon and Washington. Can. J. For. Res. https://doi.org/10.1139/cjfr-2020-0318 cjfr-2020-0318.

Roberts, David W., 2019. labdsv: Ordination and Multivariate Analysis for Ecology. R package version 2.0-1. https://CRAN.R-project.org/package=labdsv.
Rognes, T., Flouri, T., Nichols, B., Quince, C., Mahé, F., 2016. VSEARCH: a versatile open source tool for metagenomics. PeerJ 4, e2584. https://doi.org/10.7717/peerj.2584.
Roussel, J.-R., Auty, D., Coops, N.C., Tompalski, P., Goodbody, T.R.H., Meador, A.S., Bourdon, J.-F., de Boissieu, F., Achim, A., 2020. lidR: an R package for analysis of Airborne Laser Scanning (ALS) data. Remote Sens. Environ. 251, 112061. https://doi.org/10.1016/j.rse.2020.112061.
Saikkonen, K., Faeth, S.H., Helander, M., Sullivan, T.J., 1998. Fungal endophytes: a continuum of interactions with host plants. Annu. Rev. Ecol. Syst. 29, 319–343. https://doi.org/10.1146/annurev.ecolsys.29.1.319.
Scholtysik, A., Unterseher, M., Otto, P., Wirth, C., 2013. Spatio-temporal dynamics of endophyte diversity in the canopy of European ash (*Fraxinus excelsior*). Mycol. Prog. 12, 291–304. https://doi.org/10.1007/s11557-012-0835-9.
Schweiger, A.K., Lussier Desbiens, A., Charron, G., La Vigne, H., Laliberté, E., 2020. Foliar sampling with an unmanned aerial system (UAS) reveals spectral and functional trait differences within tree crowns. Can. J. For. Res. 50, 966–974. https://doi.org/10.1139/cjfr-2019-0452.
Sherwood, M., Carroll, G., 1974. Fungal succession on needles and young twigs of old-growth Douglas fir. Mycologia 66, 499–506. https://doi.org/10.1080/00275514.1974.12019631.
Sherwood-Pike, M., Stone, J.K., Carroll, G.C., 1986. *Rhabdocline parkeri* , a ubiquitous foliar endophyte of Douglas-fir. Can. J. Bot. 64, 1849–1855. https://doi.org/10.1139/b86-245.
Sillett, S.C., Rambo, T.R., 2000. Vertical distribution of dominant epiphytes in Douglas-fir forests of the central Oregon Cascades. Northwest Sci 74, 44–49.
Smirnova, E., Huzurbazar, S., Jafari, F., 2019. PERFect: PERmutation Filtering test for microbiome data. Biostatistics 20, 615–631. https://doi.org/10.1093/biostatistics/kxy020.
Spies, T., 2016. LiDAR Data (August 2008) for the Andrews Experimental Forest and Willamette National Forest Study Areas. Long-Term Ecological Research. Forest Science Data Bank, Corvallis, Oregon, USA. https://doi.org/10.6073/pasta/c47128d6c63dff39ee48604ecc6fabfc. Database.
Stone, J.K., 1987. Initiation and development of latent infections by *Rhabdocline parkeri* on Douglas-fir. Can. J. Bot. 65, 2614–2621. https://doi.org/10.1139/b87-352.
Stone, J.K., Capitano, B.R., Kerrigan, J.L., 2008. The histopathology of *Phaeocryptopus gaeumannii* on Douglas-fir needles. Mycologia 100, 431–444. https://doi.org/10.3852/07-170R1.
Sturm, M., Schroeder, C., Bauer, P., 2016. SeqPurge: highly-sensitive adapter trimming for paired-end NGS data. BMC Bioinformatics 17, 208. https://doi.org/10.1186/s12859-016-1069-7.
Taudière, A., Bellanger, J.-M., Carcaillet, C., Hugot, L., Kjellberg, F., Lecanda, A., Lesne, A., Moreau, P.-A., Scharmann, K., Leidel, S., Richard, F., 2018. Diversity of foliar endophytic ascomycetes in the endemic Corsican pine forests. Fungal Ecol 36, 128–140. https://doi.org/10.1016/j.funeco.2018.07.008.
Taylor, D.L., Walters, W.A., Lennon, N.J., Bochicchio, J., Krohn, A., Caporaso, J.G., Pennanen, T., 2016. Accurate estimation of fungal diversity and abundance through improved lineage-specific primers optimized for Illumina amplicon sequencing. Appl. Environ. Microbiol. 82, 7217–7226. https://doi.org/10.1128/AEM.02576-16.
Thers, H., Brunbjerg, A.K., Læssøe, T., Ejrnæs, R., Bøcher, P.K., Svenning, J.-C., 2017. Lidar-derived variables as a proxy for fungal species richness and composition in temperate Northern Europe. Remote Sens. Environ. 200, 102–113. https://doi.org/10.1016/j.rse.2017.08.011.
Thomas, D.C., Vandegrift, R., Ludden, A., Carroll, G.C., Roy, B.A., 2016. Spatial ecology of the fungal genus *Xylaria* in a tropical cloud forest. Biotropica 48, 381–393. https://doi.org/10.1111/btp.12273.
Unterseher, M., Tal, O., 2006. Influence of small scale conditions on the diversity of wood decay fungi in a temperate, mixed deciduous forest canopy. Mycol. Res. 110, 169–178. https://doi.org/10.1016/j.mycres.2005.08.002.
Unterseher, M., Reiher, A., Finstermeier, K., Otto, P., Morawetz, W., 2007. Species richness and distribution patterns of leaf-inhabiting endophytic fungi in a temperate forest canopy. Mycol. Prog. 6, 201–212. https://doi.org/10.1007/s11557-007-0541-1.
Valdez, J.W., Brunbjerg, A.K., Fløjgaard, C., Dalby, L., Clausen, K.K., Pärtel, M., Pfeifer, N., Hollaus, M., Wimmer, M.H., Ejrnæs, R., Moeslund, J.E., 2021. Relationships between macro-fungal dark diversity and habitat parameters using LiDAR. Fungal Ecol 51, 101054. https://doi.org/10.1016/j.funeco.2021.101054.
Wang, Q., Garrity, G.M., Tiedje, J.M., Cole, J.R., 2007. Naïve Bayesian classifier for rapid assignment of rRNA sequences into the new bacterial taxonomy. Appl. Environ. Microbiol. 73, 5261–5267. https://doi.org/10.1128/AEM.00062-07.
Wickham, H., Averick, M., Bryan, J., Chang, W., D'Agostino McGowan, L., François, R., Grolemund, G., Hayes, A., Henry, L., Hester, J., Kuhn, M., Pedersen, T.L., Miller, E., Milton Bache, S., Müller, K., Ooms, J., Robinson, D., Seidel, D.P., Spinu, V., Takahashi, K., Vaughan, D., Wilke, C., Woo, K., Yutani, H., 2019. Welcome to the tidyverse. J. Open Source Softw. 4, 1686.
Winton, L.M., Stone, J.K., Hansen, E.M., Shoemaker, R.A., 2007. The systematic position of *Phaeocryptopus gaeumannii*. Mycologia 99, 240–252. https://doi.org/10.1080/15572536.2007.11832584.
Würth, D.G., Dahl, M.B., Trouillier, M., Wilmking, M., Unterseher, M., Scholler, M., Sørensen, S., Mortensen, M., Schnittler, M., 2019. The needle mycobiome of *Picea glauca* – a dynamic system reflecting surrounding environment and tree phenological traits. Fungal Ecol 41, 177–186. https://doi.org/10.1016/j.funeco.2019.05.006.
Yan, C.-F., Han, S.-J., Zhou, Y.-M., Wang, C.-G., Dai, G.-H., Xiao, W.-F., Li, M.-H., 2012. Needle-age related variability in nitrogen, mobile carbohydrates, and δ13C within *Pinus koraiensis* tree crowns. PLoS ONE 7, e35076. https://doi.org/10.1371/journal.pone.0035076.
Zimmerman, N.B., Vitousek, P.M., 2012. Fungal endophyte communities reflect environmental structuring across a Hawaiian landscape. Proc. Natl. Acad. Sci. 109, 13022–13027. https://doi.org/10.1073/pnas.1209872109.